Spatial linear disturbances in a plane wall jet

Lars-Uve Schrader,[1, a)] Catherine Mavriplis,[1] and Luca Brandt[2]
[1)] *Department of Mechanical Engineering, University of Ottawa, Ottawa, Canada K1N 6N5*
[2)] *Linné Flow Centre, KTH Mechanics, SE-100 44 Stockholm, Sweden*

(Dated: 21 April 2012)

A two-dimensional direct numerical simulation study of the linear instability in a laminar plane wall jet is presented. The evolution of the wall jet disturbances is in reasonable agreement with predictions by spatial linear stability theory only with regard to the wavelength and the amplitude shape of the disturbance, whereas significant differences in the linear growth rate are noticed. As a consequence, the "stable island" on the instability map based on linear stability theory turns out to be connected with the outer stable region in the simulations, thus taking the form of a "stable peninsula". The failure of the theory is attributed to the rapid streamwise spread and decay of the wall jet, which is incompatible with the assumption of parallel flow. We also assess the maximum possible transient linear amplification of two-dimensional disturbances in the plane wall jet, using the concept of optimal initial disturbances. The transient energy growth relies on the Orr mechanism, and the upper bound of the disturbance energy increases linearly in time for the present flow configuration. The optimal disturbances exhibit local maxima near the edge of the jet and close to the wall, where sites of effective receptivity are hence expected. We find that the outer region of the plane wall jet is more receptive to time periodic forcing than the inner region.

I. INTRODUCTION

Consider a jet injected through a narrow spanwise slit over a wall into a quiescent fluid (Fig. 1). The fully developed flow conditions downstream of the slit are known as laminar plane wall jet. Wall jets are characterized by their maximum speed U_m and their thickness δ, defined as the wall distance where the streamwise velocity in the outer flow field is $U_m/2$. The jet speed decays as $U_m \propto x^{-1/2}$ while the thickness grows as $\delta \propto x^{3/4}$ with the downstream distance x (Ref. 1). $U_m(x)$ and $\delta(x)$ form along with the fluid viscosity ν the local Reynolds number $Re(x) = U_m(x)\delta(x)/\nu$. Laminar wall jets can be modeled using similarity theory[2,3]. The streamwise self-similar flow profiles (Fig. 2) are a fairly accurate approximation of fully developed plane wall jets observed in experiments[4]. A recent application of laminar wall jets is found in cooling devices of laptop computer processors[5].

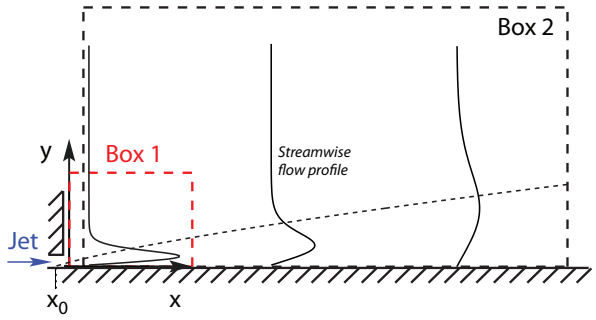

FIG. 1. Schematic of laminar plane wall jet originating in x_0. Dashed boxes depict the two computational domains considered in this study (box heights scaled up by five).

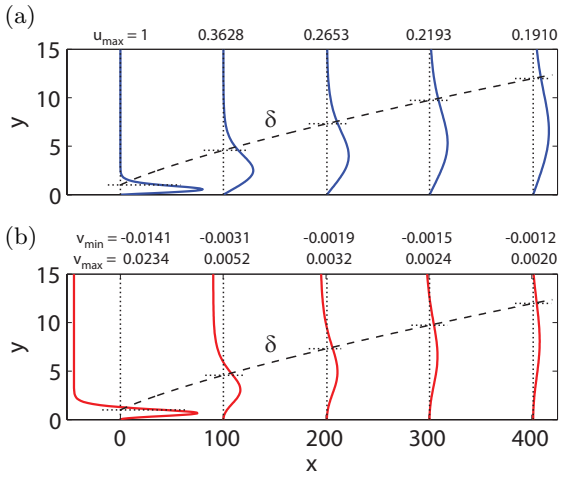

FIG. 2. Downstream development of the plane wall jet. Wall-normal profiles of (a) streamwise and (b) vertical velocity at five streamwise stations (Re = 225; 373.5; 436.8; 480.4; 514.8), along with local values of jet speed u_{max}, entrainment velocity v_{min} and wall displacement velocity v_{max}. Dashed line shows local wall jet thickness $\delta(x)$.

According to linear stability theory (LST), laminar plane wall jets become unstable beyond a critical Reynolds number of Re_c = 57 (Ref. 6; we report Re_c = 56.75 in Fig. 3). The discrete modes of the Orr-Sommerfeld/Squire spectrum of spatial eigenvalues represent two different types of instability referred to as 'mode 1' and 'mode 2'[7]. The eigenfunctions of these modes feature two local maxima of the streamwise velocity amplitude in the core of the wall jet (Fig. 4). Mode 1, becoming unstable first, assumes its global maximum near the inflection point in the outer part of the wall jet

[a)] lschrade@uOttawa.ca

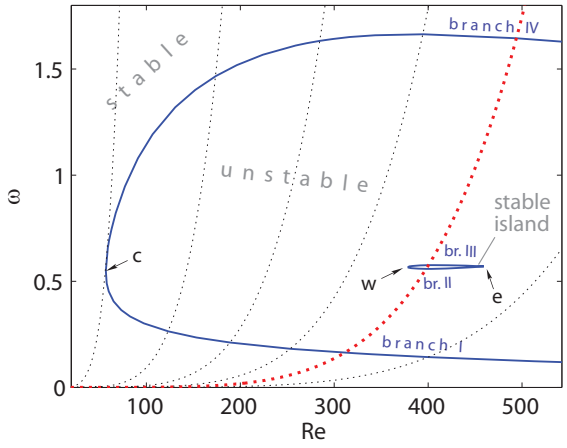

FIG. 3. Instability map of plane wall jet as per spatial LST. Neutral stability curve with four branches (I–IV). Point 'c' marks critical conditions ($Re_c = 56.75$, $\omega_c = 0.549$; critical streamwise wavenumber is $\alpha_c = 1.164$). Points 'w' and 'e' mark western and eastern tips of stable island ($Re_w = 378.25$, $\omega_w = 0.566$; $Re_e = 459.35$, $\omega_e = 0.570$). Dotted lines are trajectories of constant dimensional frequency; thick dotted line (red online) pertains to $\omega = 0.0321$ (value normalized at $Re = 225$).

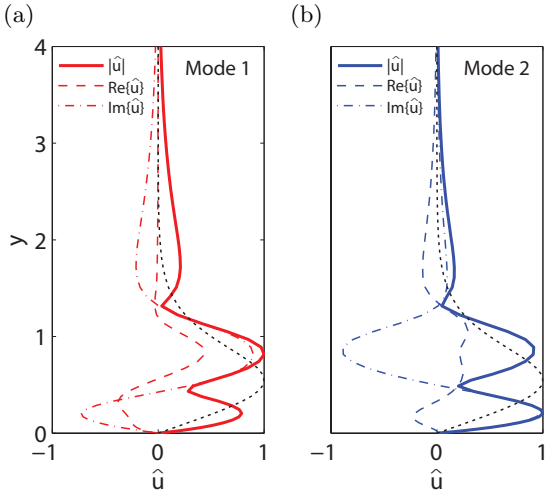

FIG. 4. Wall-normal shape of plane wall jet instability eigenmodes from spatial LST for conditions of point 'e' in Fig. 3 ($Re_e = 459.35$, $\omega_e = 0.570$). Normalized magnitude and real and imaginary parts of streamwise velocity of (a) mode 1 and (b) mode 2. Dotted line shows normalized wall jet streamwise velocity profile for comparison.

profile (Fig. 4a) where the flow is prone to inviscid instability; mode 2 is most intense near the wall (Fig. 4b) where viscous instability may occur[8]. The coexistence of these two modes leads to composite growth curves of the linear wall jet instability (Fig. 5b) and four branches of the neutral stability curve (labeled I–IV in Fig. 3), separating the regions in the instability map where mode 1 or mode 2 is unstable, or both modes are stable. The

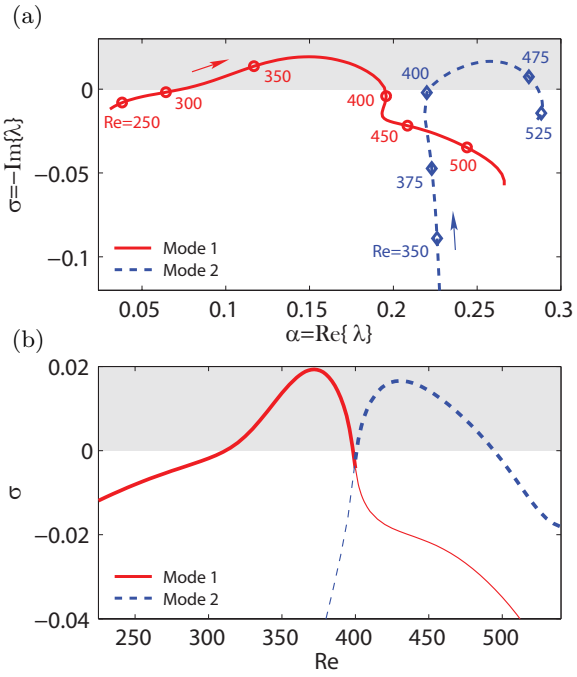

FIG. 5. (a) Trajectories of the eigenvalues λ of modes 1 and 2 on the complex plane for increasing Reynolds number. Modes follow thick dotted line (red online) in Fig. 3 ($\omega = 0.0321$). (b) Spatial growth rates $\sigma = -\mathrm{Im}\{\lambda\}$ of modes 1 and 2 versus Reynolds number. Thick portions of lines highlight composite growth curve of wall jet instability. Shaded regions indicate unstable half-plane.

latter region is not connected but features a small "stable island" within the unstable regime[6,9]. The stable island only persists in a limited range of frequencies, for which mode 1 leaves the unstable half-plane of complex eigenvalues λ before mode 2 enters it (Fig. 5a). At the lowest Reynolds number of the stable island, $Re_w \approx 381$ (Ref. 10; our finding in Fig. 3: $Re_w = 378.25$), the inviscid and the viscous modes coalesce at a fixed frequency, assuming the same streamwise wavenumber and (zero) growth rate[10]. Apart from modal instabilities, three-dimensional nonmodal disturbances may also develop in wall jets[11]. These undergo transient growth and become manifest as quasi-steady streamwise disturbance streaks in the outer part of the wall jet.

The present paper reports direct numerical simulations (DNS) of a laminar plane wall jet. We revisit the linear instability of the wall jet in order to assess the applicability and limitations of spatial LST for this flow type (Sec. III A). Optimal initial disturbances and the resulting transient growth of two-dimensional instabilities are computed (Sec. III B), and possible sites of receptivity are inferred from the shape of these optimal disturbances (Sec. III C). Time periodic localized forcing is applied at these sites in order to clarify their relevance for the receptivity of the plane wall jet.

II. SIMULATIONS

A. Flow type

A two-dimensional incompressible wall jet is studied in the Reynolds-number regime $150 \leq Re \leq 520$. The flow conditions are established by the inflow Reynolds number $Re_0 = U_{m0}\delta_0/\nu$, where the inflow values of the jet thickness and maximum speed, δ_0 and U_{m0}, are used to normalize the lengths and velocities. Two different computational domains are considered (labeled 'Box 1' and 'Box 2' in Fig. 1), with inflow Reynolds numbers of $Re_0 = 150$ (Box 1) and 225 (Box 2). The size, resolution and Reynolds number range of the two boxes are listed in Table I. Since the reference lengths and speeds are different, the normalized values of x and y pertaining to Box 1 and Box 2 are not directly comparable (see Fig. 1 for the relative size and location of the boxes).

The undisturbed flow (baseflow) is denoted by U (streamwise velocity) and V (wall-normal velocity). Two different baseflows are used: a streamwise self-similar wall jet, solution to the boundary layer equations ('BLE baseflow', cf. Fig. 2), and a wall jet fulfilling the incompressible Navier-Stokes equations ('NSE baseflow'). The NSE baseflow is obtained using self-similar wall jet profiles at the inflow and top boundaries of the DNS domain. The outer flow field is truncated at a distance of about 3.6 jet thicknesses from the wall, measured at the outlet of the computational boxes. Numerical tests with lower and higher domains reveal that the boxes chosen are high enough. No-slip and no-stress conditions are prescribed along the flat plate and the outflow boundary, respectively.

We present a brief comparison between the NSE and BLE solutions here as we will use both baseflows for the instability calculations. The downstream growth of the NSE wall jet thickness closely follows the BLE distribution $\delta(x)/\delta_0 = [(|x_0| + x)/|x_0|]^{3/4}$ (Fig. 6a, shown for Box 2), with $x_0 = -15.2$ being the virtual origin of the wall jet. The curves for the NSE and BLE baseflows are matched at the computational outflow, where the similarity approximation is most accurate. We also notice good agreement between the theoretical jet decay $U_m(x)/U_{m0} = [(|x_0| + x)/|x_0|]^{-1/2}$ and that of the NSE baseflow (Fig. 6b). However, the upstream growth of δ and decay of U_m are slightly enhanced in the NSE wall jet, causing an initially faster growing local Reynolds number as compared to the BLE baseflow (Fig. 6c). The relative difference in Re between the NSE and BLE baseflows levels out at about 3% towards the outlet (Fig. 6d), indicating that the NSE solution approaches a self-similar behavior in the downstream region. Similar results are obtained when using Box 1 (not shown).

The instability of the wall jet is computed by linear DNS (LDNS) solving the incompressible linearized Navier-Stokes equations. These govern the linear evolution of small-amplitude disturbances, where u and v denote the streamwise and wall-normal perturbation velocity components. The inflow disturbance is modeled by mode 1 or mode 2 (see Fig. 4). The disturbance is assumed to vanish along the wall and the top boundary, and a zero-stress condition is prescribed at the outlet. When solving the direct and adjoint linearized Navier-Stokes equations (Sec. III C), we use disturbance free conditions along all boundaries. These are combined with sponge regions at the computational inlet and outlet, where the direct and adjoint linear disturbances smoothly decay to zero (see Ref. 12 for the sponge technique).

TABLE I. Size of spectral element grids used ('Box 1' and 'Box 2' in Fig. 1), where x and y are streamwise and wall-normal directions (normalized by respective inflow jet thickness Boxes 1 and 2), x_0 denotes virtual origin of wall jet and Re is the Reynolds number. Values pertain to BLE baseflow.

Box	x	y	x_0	Re
1	$\in [0, 360]$	$\in [0, 55]$	-10.1	$\in [150, 369]$
2	$\in [0, 420]$	$\in [0, 45]$	-15.2	$\in [225, 520]$

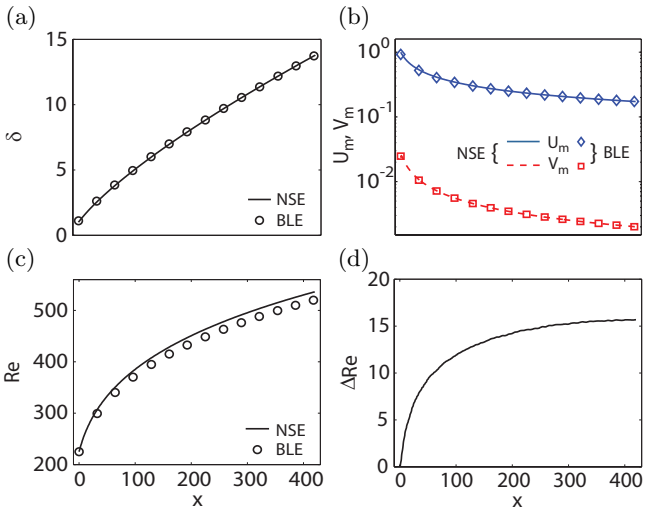

FIG. 6. Comparison between NSE and BLE baseflows for plane wall jet (Box 2, $Re_0 = 225$). Downstream development of (a) jet thickness, (b) maxima of streamwise and wall-normal velocity and (c) local Reynolds number. (d) Difference between local Reynolds number of NSE and BLE baseflows.

B. Numerical method

The DNS results on the wall jet instability are obtained by solving the two-dimensional incompressible linearized Navier-Stokes equations (LDNS) with a spectral element method (SEM)[13]. The SEM combines spectral accuracy with a flexible allocation of the grid points and is, unlike Fourier-based spectral methods, suitable for inflow-outflow problems of downstream developing flows. The spatial domain is discretized by spectral elements, which in turn are subdivided into arrays of quadrature nodes.

TABLE II. Resolution of the two spectral element grids used ('Box 1' and 'Box 2' in Fig. 1), where K_x, K_y and K are the numbers of elements in the x and y directions and in total, N is the spectral order and n_{tot} denotes the degrees of freedom.

Box	K_x	K_y	K	N	n_{tot}
1	120	28	3360	7	165677
2	140	24	3360	7	165789

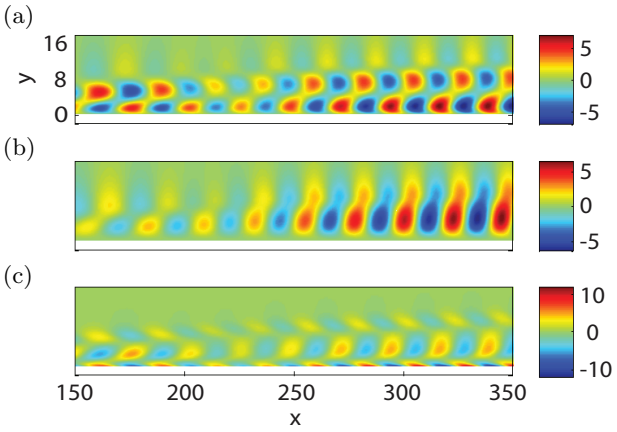

FIG. 7. Spatial structure of disturbance ($\omega = 0.0321$) in plane wall jet (Box 2, $Re_0 = 225$; y axis scaled up by two). Instantaneous fields of (a) streamwise and (b) wall-normal velocity and (c) spanwise vorticity. Results from LDNS about BLE baseflow with mode 1 as inflow disturbance.

The flow variables are approximated on the elements by tensor products of Lagrangian interpolants using Legendre polynomials. The spatial discretization is determined by the number of spectral elements, K, and the highest degree of the Legendre polynomials employed, N (see Table II). We use the open source SEM implementation Nek5000[14], optimized for MPI-based parallel computations. Numerical tests reveal that a choice of 32 MPI processors represents the best compromise between short simulation times and high efficiency for the present two-dimensional LDNS computations.

The LST calculations employ a Chebyshev collocation method with 257 nodes in order to discretize the spatial Orr-Sommerfeld/Squire operator for the plane wall jet. The vertical coordinate is truncated at the same level as that of the DNS Boxes 1 and 2 (see Table I).

III. LINEAR INSTABILITY

A. Modal Growth

We report LDNS results of the linear spatial disturbance evolution in the laminar plane wall jet. Most of the simulations presented use the BLE baseflow and inflow disturbances made up by spatial LST eigenfunctions of mode 1 type. The incoming disturbance is normalized

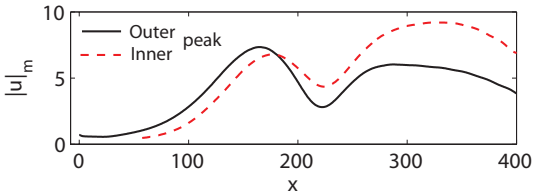

FIG. 8. Downstream evolution of disturbance ($\omega = 0.0321$) in plane wall jet computed by LDNS about BLE baseflow (Box 2, $Re_0 = 225$), using mode 1 as inflow disturbance. Outer and inner amplitude peak of streamwise disturbance velocity.

such that the quantity

$$\overline{u} = \int_0^{y_\infty} u_{rms} \mathrm{d}y \qquad (1)$$

is one at the inlet, where u_{rms} is the root-mean-square of the streamwise velocity and y_∞ denotes the distance of the top boundary from the wall. The streamwise disturbance developing from these inflow conditions preserves the double-peak shape typical of the wall jet eigenmodes as it travels downstream (Figs. 7a, 9a–c). However, the relative importance of the two peaks changes: the outer maximum dominates over the inner maximum in the upstream flow field and vice versa farther downstream (Fig. 8), indicating a changeover of the driving instability mechanism from the inviscid to the viscous type[8]. The difference of instability is also manifested in the wall-normal disturbance component, which is weak in the upstream region and intense farther downstream (Fig. 7b). The distribution of the horizontal and vertical disturbance velocities corresponds to strong, streamwise oscillating wall vorticity with two layers of counter-rotating spanwise vortices in the interior of the jet[15] (Fig. 7c). After a significant upstream growth, the wall jet disturbance starts to decay at $x \approx 170$ and then amplifies anew at $x \approx 220$ (Figs. 7, 8), as expected in light of the stable island on the instability map.

Local linear stability theory is commonly considered appropriate to characterize the qualitative behavior of small-amplitude disturbances in laminar plane wall jets[6,10]. For instance, Ref. 9 reports good agreement between the normalized disturbance shapes extracted from experimental data and those from spatial LST. This is confirmed here by comparing LDNS and LST results: especially far downstream, the amplitude functions of the streamwise and wall-normal disturbance velocities match well when normalized by their maximum (Figs. 9c,f). However, because the wall-normal flow profiles of the plane wall jet change more rapidly in the streamwise direction than in other wall-bounded flows (e.g. the flat plate boundary layer), the assumption of locally parallel flow may become inadequate for small Reynolds numbers and disturbances with large streamwise wavelengths (low frequencies). Here, we consider wall jet disturbances of mode 1 type with four different frequencies

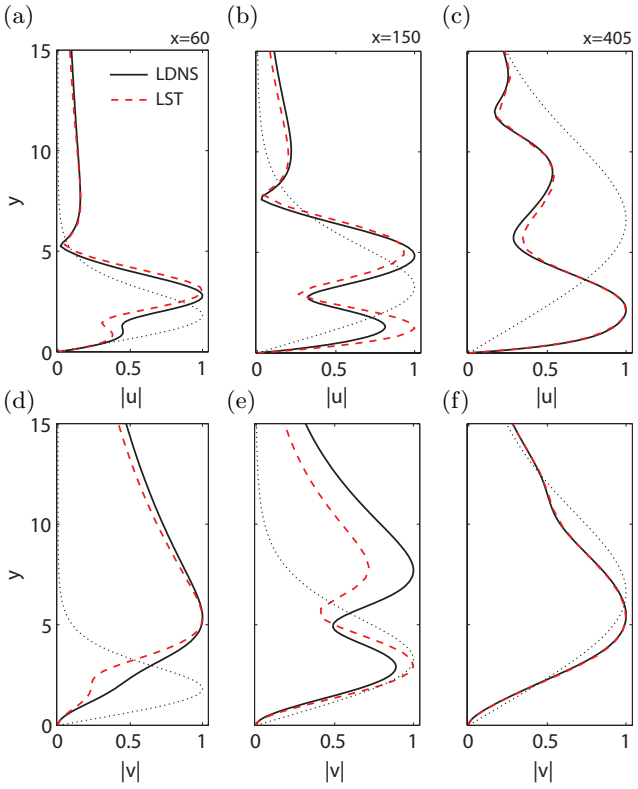

FIG. 9. Wall-normal profiles of (a,b,c) horizontal and (d,e,f) vertical disturbance velocity amplitude (normalized by maximum) in plane wall jet (Box 2, $Re_0 = 225$) for frequency $\omega = 0.0321$. Three downstream locations: (a,d) $x = 60$; (b,e) $x = 150$; (c,f) $x = 405$. Results from LDNS about BLE baseflow with mode 1 inflow disturbance and spatial LST. Thin dotted lines: normalized local wall-jet profiles for comparison.

($\omega = 0.0321$, 0.1, 0.4 and 0.8; values scaled at $Re_0 = 225$) and compare the downstream distributions of the streamwise wavenumber α and the growth rate σ obtained by LDNS and spatial LST. Both Box 1 and Box 2 are employed now, covering a fairly large portion of the ω-Re parameter space. The growth rate is calculated from the LDNS data as $\sigma = (\mathrm{d}\overline{u}/\mathrm{d}x)/\overline{u}$ (see Eq. 1 for $\overline{u}$), while the wavenumber and the growth rate of the LST computations are obtained from the real and imaginary parts of the eigenvalue λ of the spatial Orr-Sommerfeld/Squire operator, with $\alpha = \mathrm{Re}\{\lambda\}$ and $\sigma = -\mathrm{Im}\{\lambda\}$.

The strongly nonparallel streamlines of the baseflow are reflected by a rapid increase of the wavenumber α in the downstream direction (Fig. 10). The distribution of α corresponds to a large-wavelength inviscid instability upstream and a small-wavelength viscous instability downstream[9], where the region of maximum slope indicates a change in type of the most unstable eigenmode from mode 1 to mode 2. For all four frequencies, the values of α extracted from the LDNS data are in reasonable agreement with the predictions by LST. However, this does not hold for the growth rate: a large discrepancy is noticed in particular for small Reynolds numbers, where

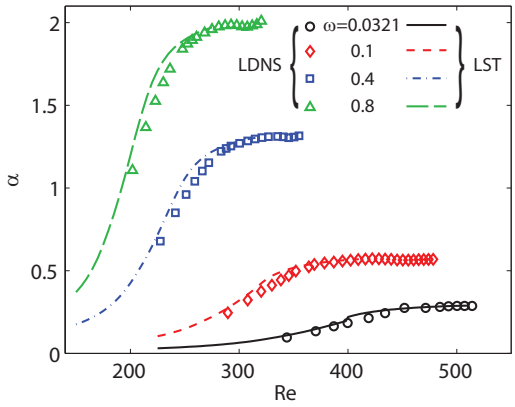

FIG. 10. Comparison of streamwise wavenumber of disturbance in plane wall jet as obtained by spatial LST and LDNS about BLE baseflow, using mode 1 as inflow disturbance. Four frequencies are considered: $\omega = 0.0321$, 0.1 (curves obtained on Box 2, $Re_0 = 225$), 0.4 and 0.8 (Box 1, $Re_0 = 150$; curves rescaled to conform to results from Box 2).

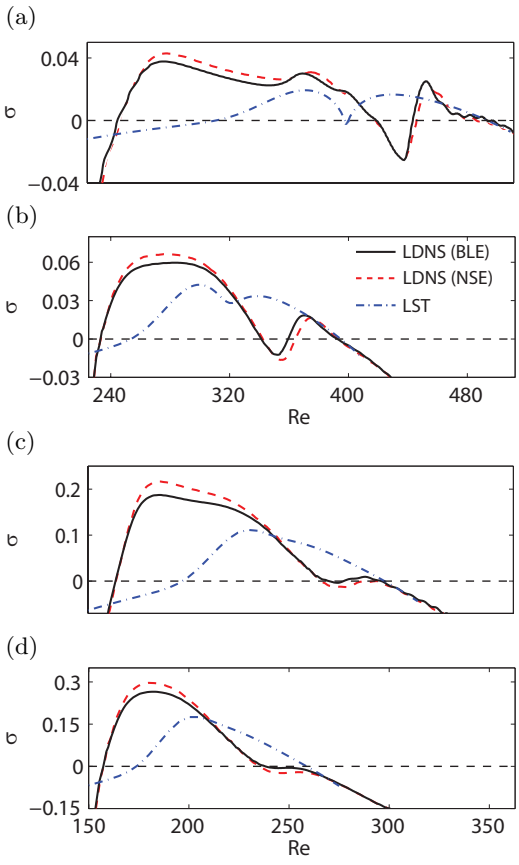

FIG. 11. Comparison of linear disturbance growth rates in plane wall jet obtained by spatial LST and LDNS about BLE and NSE baseflows, using mode 1 as inflow disturbance. Variation of frequency: (a) $\omega = 0.0321$; (b) 0.1 (curves obtained on Box 2, $Re_0 = 225$); (c) 0.4; (d) 0.8 (Box 1, $Re_0 = 150$; curves rescaled to conform to results from Box 2). Growth rate from LDNS is that of quantity $\overline{u}$ (Eq. 1).

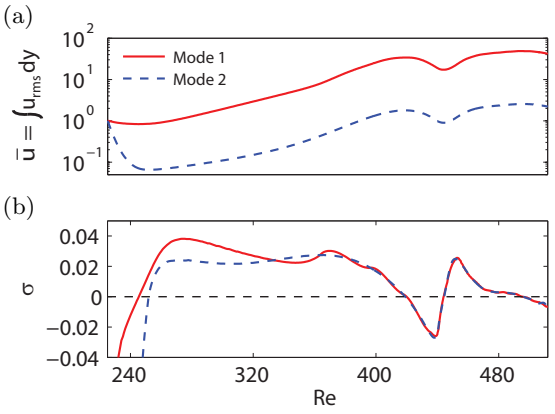

FIG. 12. Downstream disturbance evolution ($\omega = 0.0321$) in plane wall jet computed by LDNS about BLE baseflow (Box 2, $Re_0 = 225$). (a) Streamwise distribution and (b) spatial growth rate of $\overline{u}$ for two different inflow disturbances, mode 1 and mode 2.

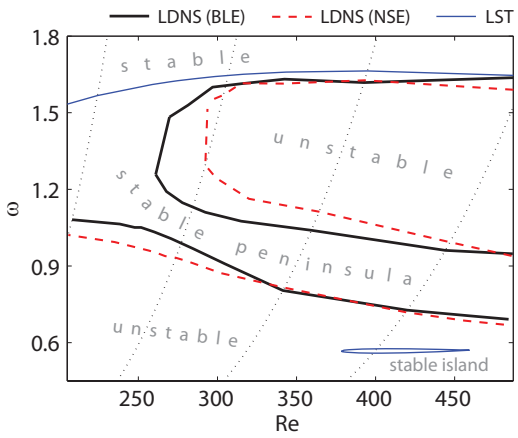

FIG. 13. Curves of neutral spatial stability of plane wall jet. Comparison between spatial LST and LDNS about BLE and NSE baseflows, using mode 1 as inflow disturbance. Thin dotted curves: lines of constant dimensional frequency.

the disturbance amplifies significantly faster in the simulations than predicted by LST (Fig. 11). According to LST, stable conditions prevail in a narrow region around $Re = 400$ for a frequency of $\omega = 0.0321$, while an extended stable patch centered at $Re \approx 439$ is observed in the LDNS data (Fig. 11a). The stable region persists and moves upstream for higher frequencies (Figs. 11b,c), whereas no stable island is seen in the LST results. At the highest frequency considered ($\omega = 0.8$, Fig. 11d), the local stable patch disappears and the wall jet disturbance becomes stable farther upstream than predicted by LST. The growth rates from LDNS and LST are consistent with each other only in the region far downstream, where the flow eventually becomes stable. The σ-distribution changes slightly when replacing the BLE baseflow (solid lines in Fig. 11) by the NSE baseflow (dashed lines, red online), especially in the upstream flow field, where the NSE baseflow deviates most significantly from the BLE solution (cf. Fig. 6d). The linear spatial development of the wall jet disturbances is hence somewhat sensitive to baseflow modifications. However, this sensitivity only contributes marginally to the disagreement between LDNS and LST, while the major contribution is attributed to the highly nonparallel nature of the plane wall jet.

We have so far only considered inflow disturbances consisting of mode 1. However, because branch IV of the neutral stability curve is established by mode 2 and branches II and III by a changeover from mode 1 to mode 2 according to LST (cf. Fig. 5), mode 2 is expected to contribute to the linear wall jet instability. Here, we compare the downstream evolution of wall jet disturbances originating from mode 1 and mode 2 inflow conditions, using the measure $\overline{u}$ (Eq. 1). Although the disturbance arising from mode 2 is more strongly damped near the inlet than that due to mode 1 (Fig. 12a, shown for $\omega = 0.0321$), the $\overline{u}$ curves become similar farther downstream so that the spatial growth rates converge at $Re \approx 390$ ($x \approx 104$, Fig. 12b). We notice that the neutral stability point pertaining to branch I is determined by mode 1, whereas the neutral points on branches II, III and IV are unaffected by the type of inflow mode chosen. This behavior, also observed for frequencies other than $\omega = 0.0321$, is explained by a mutual excitation of the modes: when prescribing mode 1 at the LDNS inlet, mode 2 is also forced and vice versa, so that the two modes appear simultaneously and are inseparable in the downstream disturbance field.

In order to clarify in what way the mismatch of the growth rates obtained by LDNS and LST affects the instability map of the plane wall jet, we report a parameter study over various frequencies in the interval $\omega \in [0.015, 1.6]$ (values normalized at $Re_0 = 225$). Because most parts of branch I of the neutral stability curve lie outside the Reynolds number range captured by the LDNS Boxes 1 and 2, the study only includes the stable island and branch IV. It is sufficient to consider inflow disturbances of mode 1 type only as branches II, III and IV do not depend on the type of inflow mode chosen (see Fig. 12). When redrawn as per the LDNS results, the instability map looks fairly different from that known from LST: the inner stable patch is shifted towards higher frequencies, covers a larger area and is connected with the outer stable region, forming a "stable peninsula" (Fig. 13). Acceptable agreement between LST and LDNS data is only obtained at branch IV for $Re \gtrsim 300$. The enlargement of the stable area in the present part of the instability map seen in the LDNS suggests a local stabilization of the wall jet owing to nonparallel effects, although the overall effect of the diverging streamlines appears to be a destabilizing one (cf. the enhanced upstream growth rates in Fig. 11). While the overall appearance of the LDNS instability diagram does not depend on the type of baseflow, the stable portion is a little larger when using the NSE solution instead of the fully self-similar

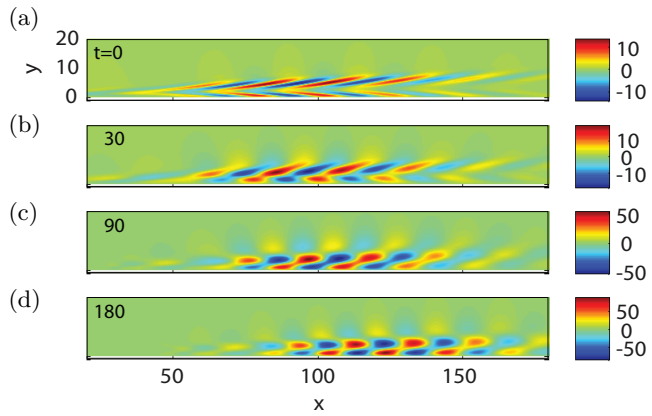

FIG. 14. Early phase of optimal disturbance evolution in plane wall jet (Box 2, $Re_0 = 225$, BLE baseflow) for growth period $T = 800$. (a) Time $t = 0$, (b) 30, (c) 90 and (d) 180.

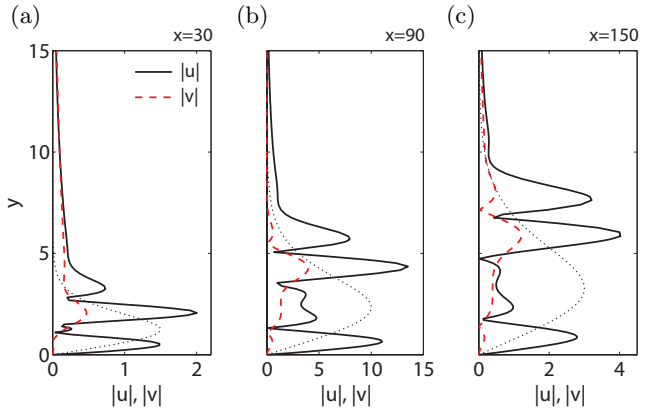

FIG. 15. Wall-normal profiles of streamwise and wall-normal velocity magnitude of optimal disturbance shown in Fig. 14(a) at three downstream locations: (a) $x = 30$, (b) 90, (c) 150. Thin dotted lines: wall-jet profiles (BLE baseflow) at the same locations, scaled for comparison.

BLE baseflow. Although the neutral stability curve from LDNS somewhat changes when tracking the growth rates of other quantities than $\overline{u}$, e.g. the disturbance energy or the streamwise velocity at the inner and outer peaks of the disturbance profile, the principal topography of the LDNS instability map remains the same.

B. Transient Growth

Shear flows are known to support short-time amplification of nonmodal disturbances. Here, we study the potential of linear transient growth in the laminar plane wall jet using the concept of 'optimal disturbances'. These are initial flow structures evolving into a disturbance pattern with maximum kinetic energy at a certain time T. The disturbance kinetic energy is defined as

$$E(t) = \frac{1}{L_x L_y} \int_0^{L_x} \int_0^{L_y} \mathbf{u}(t)^2 \mathrm{d}y\mathrm{d}x, \qquad (2)$$

where t denotes the time, $\mathbf{u} = (u, v)$ is the disturbance velocity and $L_x = 420$ and $L_y = 45$ are the length and height of the computational domain (Box 2). The maximum of $E(T)$ is computed using the method of Lagrange multipliers. The optimization procedure adopted employs an iterative scheme of alternating LDNS and adjoint LDNS ('timestepper technique'[16]) and is outlined in Ref. 17. The first LDNS of the iteration loop is initialized by a disturbance field with a random spatial distribution (see Ref. 18 for a schematic of the iteration procedure).

The optimal initial disturbance obtained is an upstream localized pattern of tilted structures arranged in two rows, one near the wall and the other in the outer part of the wall jet (Fig. 14a, shown for $T = 800$). These structures initially "lean against" the mean shear of the wall jet and then rotate due to shearing (Figs. 14a-c) until a pattern typical of a wall jet disturbance is achieved

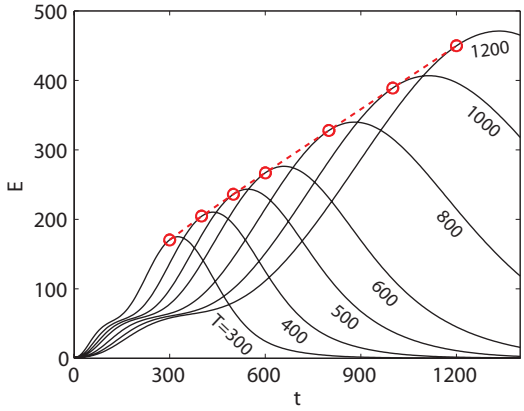

FIG. 16. Temporal evolution of disturbance kinetic energy (Eq. 2) of various optimal disturbances with $E(0) = 1$ in plane wall jet (Box 2, $Re_0 = 225$, BLE baseflow). Circles: maximum kinetic energy for different growth periods T; dashed line (red online): envelope curve.

(Fig. 14d). This process is the well-known Orr mechanism earlier reported for Couette flow, plane Poiseuille flow and the flat plate boundary layer[17,19]. In the plane wall jet, the Orr mechanism is active in two layers with mean flow gradients of opposite sign (the wall-bounded and the free shear layers), so that the inner and outer initial optimal flow structures rotate in opposite directions. The wall-normal profiles extracted from the optimal initial disturbance field exhibit a streamwise velocity magnitude with multiple local peaks and a global maximum in the outer part of the wall jet (Fig. 15).

The potential of transient growth in the plane wall jet is demonstrated by a parameter study over different growth periods T. We consider values in the range $300 \leq T \leq 1200$, for which both the optimal initial disturbance and the final wall jet instability remain inside the computational domain at all times. All optimal per-

TABLE III. Parameters of streamwise volumetric force f_x (Eq. 3). The four parameter sets listed pertain to forcing at two distances from the wall and two streamwise positions.

a_f	ω_f	x_c	y_c	b_x	b_y
1	0.0321	15	0.33 1.67	0.5	20
1	0.0321	220	1.52 7.81	0.5	20

turbations undergo rapid initial amplification followed by a 'plateau', a second phase of amplification and final decay (Fig. 16). The initial growth, ascribed to the Orr mechanism, is terminated when the plateau is reached and establishes the gain of the optimally excited unstable wavepackets with respect to purely modal wall jet instabilities ($\approx$ 50 here). The growth phase following the plateau is driven by the inviscid and viscous instability mechanisms of the plane wall jet. The maximum possible values of the disturbance kinetic energy for different growth periods T (circles in Fig. 16) group along a straight line ('envelope curve'), setting an upper bound for the linear temporal amplification of two-dimensional disturbances in the plane wall jet.

C. Receptivity

Since the optimal streamwise disturbance velocity exhibits local maxima both in the inner and the outer part of the plane wall jet (cf. Fig. 15), both regions are expected to be potentially receptive to forcing. A simple numerical experiment is carried out to clarify the region in which the wall jet is more effectively destabilized. To this end, a localized, time-periodic volumetric force is added to the linearized streamwise momentum equation,

$$f_x(x,y,t) = a_f \; e^{-[b_x(x-x_c)^2+b_y(y-y_c)^2]} \; \sin(\omega_f t), \qquad (3)$$

where a_f is the amplitude and ω_f the frequency of the forcing. A two-dimensional Gaussian distribution centered at (x_c, y_c) defines the spatial structure of the force, with b_x and b_y determining the degree of localization. We consider four sets of parameters with different centers (x_c, y_c) of the Gaussian, placed upstream ($x_c = 15$) or downstream ($x_c = 220$) and in the inner or outer part of the wall jet (see Tab. III). The inner and outer wall distances y_c are adjusted such that the local wall jet speed is $U(x_c, y_c) = U_m(x_c)/2$ in all cases. The values of b_x and b_y chosen ensure that the spatial forcing distribution is comparable to the flow structures in size.

The disturbance attains the largest amplitude, if the flow is forced near the edge of the wall jet (Fig. 17, shown for $\omega = 0.0321$). This also holds if the force is applied farther downstream ($x_c = 220$) where the inner peak of the wall jet disturbance amplitude is dominant (see Fig. 8). The larger receptivity of the outer wall jet region is consistent with the outer location of the global maximum of the optimal disturbances (cf. Fig. 15). In practice, plane wall jets are often destabilized by perturbations originating from the jet nozzle, e.g. due to a rough nozzle surface. The present results suggest that the upper nozzle wall (opposing the flat plate) is a particularly relevant site of such perturbations.

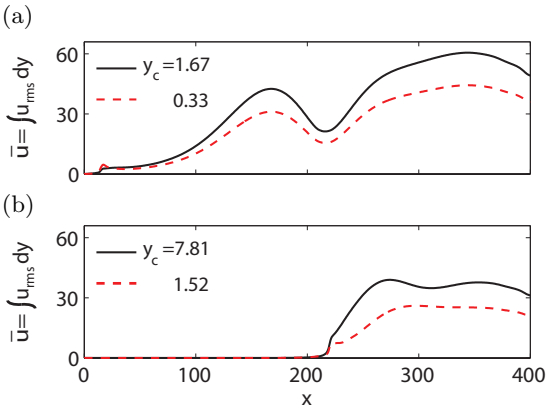

FIG. 17. Excitation of plane wall jet instability (Box 2, $Re_0 = 225$, BLE baseflow) by time periodic volumetric forcing (see Eq. 3 and Table III). Forcing is applied at two wall distances y_c in outer and inner region of wall jet and at two streamwise stations: (a) $x_c = 15$ and (b) $x_c = 220$.

IV. SUMMARY

A two-dimensional direct numerical simulation (DNS) study of a laminar plane wall jet is presented. Previous DNS studies of this flow type deal with transition to turbulence[20], nonlinear phenomena[21] and forced heat transfer[22]. In this work, we focus on the linear evolution of disturbances in the plane wall jet and compare results from linear DNS (LDNS) and spatial linear stability theory (LST). Ref. 9 reports fair agreement of the normalized streamwise disturbance velocity profiles when data from experiments and LST are matched. Our comparison between LDNS and LST data confirms this, and we also notice reasonable agreement of the disturbance wavelengths. This is in line with Ref. 23, where satisfactory LST calculations of normalized disturbance profiles and wavelengths in flat plate boundary layers are reported. However, LST results of the spatial disturbance growth rates in the plane wall jet turn out to be inaccurate. At low Reynolds numbers, the instabilities amplify significantly faster in the simulations than predicted by LST. The growth rates only agree near the downstream branch of the neutral stability curve (branch IV), where the disturbances eventually decay.

Our LDNS results imply a modified instability map of the plane wall jet: the stable island predicted by LST appears to be significantly larger than reported so far[6,9,10]

and is connected with the outer stable region, forming a "stable peninsula". We attribute the failure of LST to the rapid streamwise variation of the wall jet (as compared with e.g. the flat plate boundary layer), which is incompatible with the parallel flow assumption and the requirement of sufficiently separated characteristic length scales of the baseflow and the unstable eigenmodes. The overall nonparallel effect is manifested as a destabilization of the plane wall jet, as shown before in flat plate boundary layers[23], while the flow is locally stabilized in the neighborhood of the stable peninsula. We anticipate that the rapid streamwise evolution of the wall jet also affects the lowest branch of the neutral stability curve (branch I) and possibly the critical Reynolds number of linear instability. However, we have not verified this as the long disturbance waves at the critical conditions along with the excessive spreading rate of the wall jet would require costly simulations on large domains beyond the scope of this study. Moreover, the self-similar approximation would become inadequate in the near field of the wall jet, which strongly depends on the geometry of the jet orifice.

We also report the transient growth potential of two-dimensional disturbances in the plane wall jet, using the concept of 'optimal disturbances'. These are computed by an iterative procedure of direct and adjoint Navier-Stokes simulations (timestepper technique[16]). The optimal initial disturbances consist of upstream tilted flow structures similar to those in flat plate boundary layers[17,19] – but in the wall jet, these structures are arranged in *two* rows as there are two shear layers. The tilted structures are turned by the mean shear (Orr mechanism) and evolve into traveling wavepackets. The transient evolution curves for different growth times establish a straight envelope line. The wall-normal profiles of the optimal streamwise disturbance velocity exhibit multiple local maxima across the wall jet, explaining the large receptivity to perturbations and the rapid destabilization of this flow type. The excitation of wall jet instabilities by localized volumetric forcing is particularly effective in the outer region of the plane wall jet, where the baseflow appears to be more receptive than near the wall.

ACKNOWLEDGMENTS

The authors wish to acknowledge Dr. Antonios Monokrousos for generously providing the adjoint Navier-Stokes solver of the spectral element code. This research is funded by the Natural Sciences and Engineering Research Council of Canada (NSERC). Computing time by the Swedish National Infrastructure for Computing (SNIC) is gratefully acknowledged.

[1]N. Tetervin. Laminar flow of a slightly viscous incompressible fluid that issues from a slit and passes over a flat plate. Technical Report TN 1644, NACA, 1948.

[2]N. I. Akatnov. Development of two-dimensional laminar incompressible jet near a rigid wall. In *Proc. Leningrad Polytech. Inst. (Trudy LPI)*, volume 5, pages 24–31. Mashinostroenie, Moscow, 1953. ISSN 0376-1304.

[3]M. B. Glauert. The wall jet. *J. Fluid Mech.*, 1:625–643, 1956.

[4]R. A. Bajura and A. A. Szewczyk. Experimental Investigation of a Laminar Two-Dimensional Plane Wall Jet. *The Phys. Fluids*, 13 (7):1653–1664, 1970.

[5]R. Mongia, A. Bhattacharya, and H. Pokharna. Skin cooling and other challenges in future mobile form factor computing devices. *Microelectronics Journal*, 39 (7):992–1000, 2008.

[6]D. H. Chun and W. H. Schwarz. Stability of the Plane Incompressible Viscous Wall Jet Subjected to Small Disturbances. *The Phys. Fluids*, 10 (5):911–915, 1967.

[7]A. Tumin. Subharmonic resonance in a laminar wall jet. *Phys. Fluids*, 10 (7):1769–1771, 1998.

[8]P. Mele, M. Morganti, M. F. Scibilia, and A. Lasek. Behavior of Wall Jet in Laminar-to-Turbulent Transition. *AIAA Journal*, 24 (6):938–939, 1985.

[9]M. D. Zhou, J. Rothstein, and I. Wygnanski. On the hydrodynamic instability of the wall jet. In M. R. Davis, editor, *Proc. 11th Australasian Fluid Mech. Conf.*, pages 407–410, University of Tasmania, Hobart, Australia, 1992. ISSN 0814-8007.

[10]A. Tumin and L. Aizatulin. Instability and Receptivity of Laminar Wall Jets. *Theoret. Comput. Fluid Dynamics*, 9:33–45, 1997.

[11]O. Levin, V. G. Chernoray, L. Löfdahl, and D. S. Henningson. A study of the Blasius wall jet. *J. Fluid Mech.*, 539:313–347, 2005.

[12]D. Tempelmann, L.-U. Schrader, A. Hanifi, L. Brandt, and D. S. Henningson. Numerical study of boundary-layer receptivity on a swept wing. *AIAA Paper*, (2011-3294):1–13, 2011.

[13]A. T. Patera. A Spectral Element Method for Fluid Dynamics: Laminar Flow in a Channel Expansion. *J. Comp. Phys.*, 54:468–488, 1984.

[14]P. Fischer, J. Kruse, J. Mullen, H. Tufo, J. Lottes, and S. Kerkemeier. *NEK5000 - Open Source Spectral Element CFD solver*. Argonne National Laboratory, Mathematics and Computer Science Division, Argonne, IL, USA. (available as of April, 2012, at https://nek5000.mcs.anl.gov/index.php/MainPage website).

[15]F. B. Hsiao and S. S. Sheu. Double row vortical structures in the near field of a plane wall-jet. *Exps. Fluids*, 17:291–301, 1994.

[16]D. Barkley, H. M. Blackburn, and S. J. Sherwin. Direct optimal growth analysis for timesteppers. *Itn. J. Numer. Meth. Fluids*, 57:1435–1458, 2008.

[17]A. Monokrousos, E. Åkervik, L. Brandt, and D. S. Henningson. Global optimal disturbances in the Blasius boundary-layer flow using time-steppers. *J. Fluid Mech.*, 650:181–214, 2010.

[18]A. Monokrousos. *Optimisation and control of shear flows*. PhD thesis, Royal Institute of Technology (KTH), Stockholm, Sweden, 2011.

[19]K. M. Butler and B. F. Farrell. Three-dimensional optimal perturbations in viscous shear flow. *Phys. Fluids A*, 4:1637–1650, 1992.

[20]R. A. Bajura and M. R. Catalano. Transition in a two-dimensional plane wall jet. *J. Fluid Mech.*, 70 (4):773–799, 1975.

[21]S. Wernz and H. F. Fasel. Nonlinear resonances in a laminar wall jet: ejection of dipolar vortices. *J. Fluid Mech.*, 588:279–308, 2007.

[22]J. Seidel and H. F. Fasel. Numerical investigations of heat transfer mechanisms in the forced laminar wall jet. *J. Fluid Mech.*, 442:191–215, 2001.

[23]H. Fasel and U. Konzelmann. Non-parallel stability of a flat-plate boundary layer using the complete Navier-Stokes equations. *J. Fluid Mech.*, 221:311–347, 1990.